Journal Name

ARTICLE TYPE

Cite this: DOI: 10.1039/xxxxxxxxxx

Laplacian of the Hamiltonian Kinetic Energy Density as an Indicator of Binding and Weak Interactions.

Pablo Carpio-Martínez,[a,b] José E. Barquera-Lozada,[a] Angel Martín Pendás,[c] and Fernando Cortés-Guzmán*[a,d]

Received Date
Accepted Date

DOI: 10.1039/xxxxxxxxxx

www.rsc.org/journalname

The kinetic energy is the center of a controversy between two opposite points of view about its role in the formation of a chemical bond. One school states that a lowering of the kinetic energy associated with electron delocalization is the key stabilization mechanism of covalent bonding. In contrast, the opposite school holds that a chemical bond is formed by a decrease in the potential energy due to a concentration of electron density within the binding region. In this work we present the topographic analysis of the Hamiltonian Kinetic Energy Density (KED) and its laplacian to gain more insight into the role of the kinetic energy within chemical interactions. Our study is focused on atoms, diatomic and organic molecules, along with their dimers. We show that the laplacian of the Hamiltonian KED exhibits a shell structure in atoms and that their outermost shell merge when a molecule is formed. Moreover, we observe that a covalent bond is characterized by a concentration of kinetic energy, potential energy and electron densities along the internuclear axis. In the case of weak intermolecular interactions, the external shell of the molecules merge into each other resulting in an intermolecular surface comparable to that obtained by the Non-covalent interaction (NCI) analysis.

1 Introduction

The controversial role of the kinetic energy (KE) in the formation of a chemical bond is still the center of a debate. There exist two different points of view concerning the role that KE plays in the evolution of chemical bonds. One view, proposed by Hellmann,[1] and supported by Peierls,[2] Platt,[3] Ruedenberg,[4;5;6;7;8;9] and Kutzelnigg,[10;11;12] states that a lowering of the kinetic energy associated with electron delocalization is the key stabilization mechanism of covalent bonding. In contrast, the opposite view, presented by Slater[13] and supported by Feynman,[14] Coulson[15] and Bader,[16;17] holds that a chemical bond is formed by a decrease in the potential energy due to a concentration of electron density within the binding region. Recently, Ruedenberg, Bacskay and Nordholm have followed this controversy by examining H_2 and H_2^+ molecules in which the virial theorem does not hold. Their findings lead to the conclusion that the phenomenon of bonding is not limited to systems with Coulombic interactions and support the idea that the kinetic energy offers a fundamental description of bonding.[18] In this work, we present a topological analysis of the Laplacian of Hamiltonian kinetic energy density to gain more insight into the role of the kinetic energy within chemical interactions, specifically non-covalent interactions.

1.1 The kinetic energy density

Classically, the local kinetic energy of a system can be defined without ambiguity, however, in quantum mechanics there exist

[a] *Instituto de Química, Unversidad Nacional Autónoma de México, México DF 04510, México.*
[b] *Department of Chemistry, University of Alberta, Edmonton, Alberta AB T6G 2G2, Canada*
[c] *Departamento de Química Física y Analítica, Facultad de Química, Universidad de Oviedo, E-33006-Oviedo, Spain.*
[d] *Centro Conjunto de Investigación en Química Sustentable UAEMex-UNAM, carretera Toluca-Atlacomulco km 14.5, Toluca, México 50200.*

† Electronic Supplementary Information (ESI) available: [details of any supplementary information available should be included here]. See DOI: 10.1039/b000000x/

‡ Additional footnotes to the title and authors can be included *e.g.* 'Present address:' or 'These authors contributed equally to this work' as above using the symbols: ‡, §, and ¶. Please place the appropriate symbol next to the author's name and include a `\footnotetext` entry in the the correct place in the list.

an infinite number of expressions that integrated over the whole space recover the total kinetic energy of the system. Most of these expressions are valid and are mathematically justified nevertheless, their conceptual usefulness is limited.[19;20] Besides, based on the way the local kinetic energy is formulated, the spatial variation of the total energy is controlled by either the kinetic or potential energy.[21] There exist several ways to generate a family of Kinetic Energy Densities (KED), but the most useful in chemistry comes from the additive multiple of the Laplacian of the electron density *i.e.*, the Laplacian family, defined as

$$\tau_\alpha(\mathbf{r}) = \tau_+(\mathbf{r}) + \left(\frac{\alpha-1}{4}\right)\nabla^2\rho(\mathbf{r}), \tag{1}$$

where $\tau_+(\mathbf{r})$ is the positive-definite kinetic energy density, which equals $\tau_1(\mathbf{r})$ when $\alpha = 1$, also denoted as $G(\mathbf{r})$. When $\alpha = 0$, one obtains the Schrodinger or Hamiltonian form, $K(\mathbf{r})$. The expressions for these two KEDs are

$$G(\mathbf{r}) = \frac{\hbar^2}{2m}N\int d\tau' \nabla\Psi^* \cdot \nabla\Psi, \tag{2}$$

$$K(\mathbf{r}) = \frac{-\hbar^2}{4m}N\int d\tau' \left[\Psi^*\nabla^2\Psi + \Psi\nabla^2\Psi^*\right]. \tag{3}$$

The difference between these two functions emerges when one examines their local behavior. $G(\mathbf{r})$ is finite and positive in all points of the space and is, in general, a monotonic function in atoms. This convenient feature makes it easily tractable up to the point that is currently the most studied out of the two functions; however, its use as a chemical descriptor is still limited due to its lack of structure.[22;23;24] In contrast $K(\mathbf{r})$ can give rise to either positive and negative values opening the possibility to extract more information about chemical interactions.[25] Locally, these functions are related by the Laplacian of the electron density according to the following equation

$$K(\mathbf{r}) = G(\mathbf{r}) + L(\mathbf{r}), \tag{4}$$

where

$$L(\mathbf{r}) = -\frac{1}{4}\nabla^2\rho(\mathbf{r}). \tag{5}$$

The topology of $G(\mathbf{r})$ and $K(\mathbf{r})$ have been studied separately by Noorizadeh[26] and Tachibana *et al.*,[27] respectively. In both cases a partition of the space was performed on the basis of the corresponding gradients, $\nabla G(\mathbf{r})$ and $\nabla K(\mathbf{r})$, resulting in atomic basins separated by zero flux surfaces, equivalent to those obtained with the electron density.

There are several examples of the application of Kinetic Energy Densities to understand chemical bonding. A very valuable tool for analyzing the phenomenon of covalent bonding based on the KED has been presented by Schmider and Becke,[28] the so-called Localized Orbital Locator (LOL). LOL enables the mapping of regions characterized by relatively slow-moving electrons and therefore, regions where KED is decreased. Based on the fact that one of the driving forces for covalent bonding is the maximum decrease of the KED, such regions can be interpreted as indicative of covalent bonding.[29] Jacobsen argues that "a description of chemical bonding based on charge densities finds the essence of a chemical bond in answer to the question where electrons are, while kinetic energy densities focus on where electrons stay." Additionally, Jacobsen has reported the complete topologies of LOL for various sets of molecules revealing patterns in chemical bonding such as Kinetic connection lines that define the extension of the valence space around an atomic center.[23] The empirical concept of the steric effect has been defined as a "kinetic energy pressure" in atoms and molecules.[30] Frank De Proft *et al.* introduced Weizsäcker kinetic energy as a measure of the steric energy, giving reasonable linear relationships with experimental evidence.[31]

Tachibana *et al.* used KED to identify the intrinsic shape of the reactants, the electronic transition state, and the reaction products along the course of a chemical reaction coordinate. Three atomic regions were identified based on a classical interpretation of the kinetic energy. $K(\mathbf{r} > 0)$, (K_A), where the electron density is amply accumulated, and motion of electrons is guaranteed. $K(\mathbf{r} < 0)$, (K_F), where the motion of electron is classically forbidden and $K(\mathbf{r} = 0)$, (K_S), the boundary between the two previous regions, which gives the shape of the atoms involved in the reaction process.[32;33] During a reaction, two K_A disjoint regions of neighboring atoms gradually polarized toward the internuclear region until they fuse, where the transition state can be identified with the coalescent point.

In the Quantum Theory of Atoms in Molecules (QTAIM),[34] a quantum atom is defined as a molecular fragment with a well defined kinetic energy.[35;36;37;38] Following the advent of QTAIM, several scalar and vector fields have been proposed to understand and predict the nature of chemical interactions. Recently, all such studies and methodologies were encompassed by the so-called Quantum Chemical Topology (QCT).[39] Some examples include, the electron density,[40] its gradient and its Laplacian,[41;42] the Electron Localization Function (ELF),[43] the Electron Localizability Indicator (ELI),[44] the Reduced Density Gradient (NCI),[45] the magnetically induced current density and its vorticity,[46;47] among others.[48] Most of the quantities used within the QCT are derived from one- and two-electron densities, meaning that the energetic properties are usually obtained by integrating densities over real space domains and not by examining appropriate energetic scalar or vector fields.[49] Besides, the scalar fields associated with energetic properties as the kinetic and potential energy densities have not been explored sufficiently.[50] Then this work aims to present the topology of the Hamiltonian KED and its Laplacian, which is related to the electronic energy density by the local virial theorem,[51;36] and their application to analyze chemical interac-

tions. The present paper is organized as follows: In section 2, we provide details of our calculations. In section 3, we discuss our results in the following order: the hydrogen atom, hydrogen molecule, diatomic molecules, organic molecules, and weak interactions. Finally, the conclusions are given in section 4.

2 Computational details

We calculated the Hamiltonian KED ($K(\mathbf{r})$) and its laplacian ($\nabla^2 K(\mathbf{r})$) for selected atoms (from H to Ca), four diatomic molecules (H_2, N_2, CO, and LiF), five organic molecules (methane, ethane, ethylene, acetylene and benzene) and their respective dimers. Analytic expressions for the two scalar fields were obtained for the hydrogen atom. The calculations were performed with Slater-type Orbitals (STOs) alongside with M06-2X DFT functional[52] with ADF2013 program.[53] The $\rho(\mathbf{r})$, $\nabla^2\rho(\mathbf{r})$ and $G(\mathbf{r})$ were obtained in 3D grids with the Dgrid code[54] and used to calculate $K(\mathbf{r})$ as described by the equation 4. $\nabla^2 K(\mathbf{r})$ was calculated numerically with a script written in python and pvpython, implemented in Paraview 4.2. Several grid spacings were tested to calculate the numerical derivatives. H atom and H_2 molecule needed very fine grids (0.005 a.u.) to achieve well converged results. Other atoms just needed coarse grids (0.02 a.u.) and their corresponding graphics were generated with a 0.01 a.u. spacing. For comparison, in some cases we calculated the same properties with Gaussian-type orbitals (GTOs) using the Gaussian 09 package[55] and AIMALL program.[56]

3 Results and discussion

3.1 The hydrogen atom

In the first place, we derived the analytic expressions of $K(\mathbf{r})$ and $\nabla^2 K(\mathbf{r})$ for the hydrogen atom. For that purpose, we used equation 3 and the wave function $\psi_{1s} = (1/\sqrt{\pi})e^{-r}$ to obtain the following equations:

$$K(\mathbf{r}) = \frac{1}{2\pi}\left(\frac{2}{r} - 1\right)e^{-2r} \tag{6}$$

$$\nabla^2 K(\mathbf{r}) = -\frac{2}{\pi}\left(1 - \frac{3}{r}\right)e^{-2r}. \tag{7}$$

The profiles of $K(\mathbf{r})$ and $\nabla^2 K(\mathbf{r})$ are shown in Figure 1 (black lines) to illustrate their behavior as a function of the distance from the nucleus. Both curves exhibit a decrease from its cusp (centered at the nucleus position, r = 0 a.u.) to a minimum, then an asymptotic increase to zero as the distance tends to infinity. The intersection with the abscissa is 2.0 a.u. for $K(\mathbf{r})$ and 3.0 a.u. for $\nabla^2 K(\mathbf{r})$. It can be seen that all the basis sets capture the behaviour of the analytic expression of $K(\mathbf{r})$; on the contrary, for $\nabla^2 K(\mathbf{r})$ the STO basis set performs better than GTO one.

It is worth mentioning that Figure 1 only displays a section

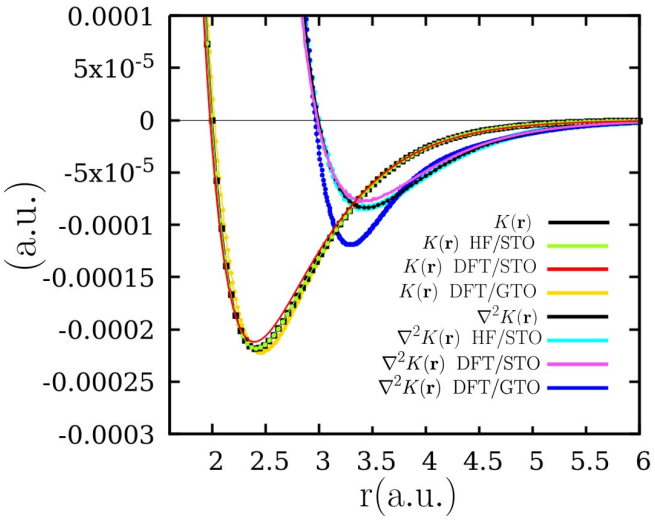

Fig. 1 Profiles of the exact expressions of $K(\mathbf{r})$ and $\nabla^2 K(\mathbf{r})$ for the hydrogen atom.

of the valence region given that the core of the atoms presents many unwanted oscillations between 0 and 0.5 a.u. due to the use of the sixth-order derivative of the electron density. The Slater basis set does not show this inconsistency around the core, and conversely, the obtained profiles agree reasonably well with the analytic ones. Outside this region, both, Slater and Gaussian basis sets give similar results.

3.2 Atoms

We computed $K(\mathbf{r})$ and $\nabla^2 K(\mathbf{r})$ for He and the subsequent atoms up to Ca. We found that, for polyelectronic atoms, $K(\mathbf{r})$ and $\nabla^2 K(\mathbf{r})$ present a shell structure similar to other scalar fields: $\nabla^2\rho(\mathbf{r})$,[41;42] ELF,[43] LOL,[28] among others. Figure 2 shows an idealized profile of $K(\mathbf{r})$ (or $\nabla^2 K(\mathbf{r})$) of an atom in the third period of the periodic table. This plot aims to characterize the topography of $K(\mathbf{r})$ and $\nabla^2 K(\mathbf{r})$ by identifying the following features: nodes (j_i), maxima and minima (α_i and β_i) and their corresponding radii (r_{α_i} and r_{β_i}). It should be noted that r_c represents the limit of the core region where the anomalous behavior occurs if GTOs are used. The numerical values associated to these values are shown in Tables 1 and 2. For $K(\mathbf{r})$, H and He atoms exhibit one α_1 shell, whereas the atoms from Li to Ar exhibit two shells (α_1 and α_2). The exceptions of this behavior are Ne and Cl atoms, which only present the α_2 shell. From the analysis of $\nabla^2 K(\mathbf{r})$, it is possible to observe that H and He have just one concentration shell of $K(\mathbf{r})$, whereas the atoms from Li to Ne have two shells and subsequently, the atoms in the third period have three shells. In contrast to $K(\mathbf{r})$, $\nabla^2 K(\mathbf{r})$ behaves well since every expected shell is observed with no exceptions.

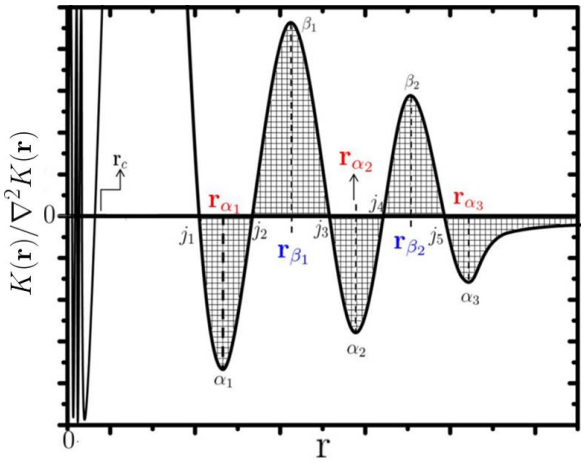

Fig. 2 Ideal profile of both $K(\mathbf{r})$ and $\nabla^2 K(\mathbf{r})$ of an atom in the third period. The origin is situated at the position of the nucleus and r represents an arbitrary axis. For the case of $K(\mathbf{r})$ the number of shells is limited to two.

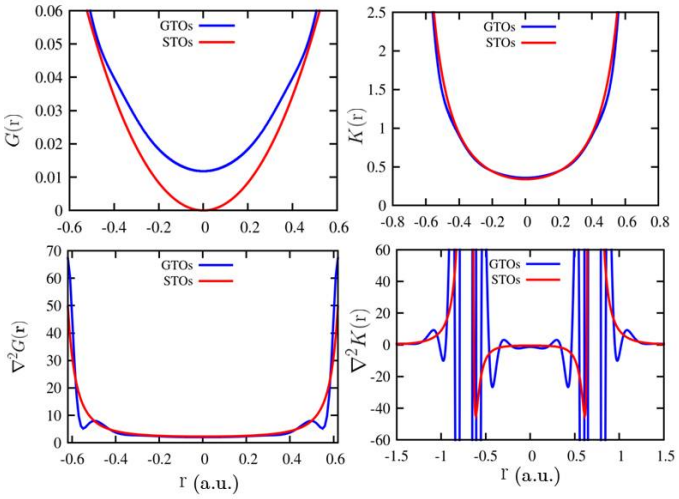

Fig. 3 Profiles of $G(\mathbf{r})$, $K(\mathbf{r})$ and their respective laplacians functions at the equilibrium geometry of hydrogen molecule.

3.3 Hydrogen molecule

Ruedenberg, Bacskay, and Nordholm described the shape of the HKED in the bonding region of H_2^+ [57] whereas Preston and Bader examined the relationship between the topographical features of charge distribution and the kinetic energy of hydrogen molecule. [25] Figure 3 shows the profiles of $K(\mathbf{r})$, $G(\mathbf{r})$, $\nabla^2 G(\mathbf{r})$ and $\nabla^2 K(\mathbf{r})$ along the internuclear axis of the equilibrium geometry of the H_2. As described by the previous reports, within the internuclear region, the behavior of $G(\mathbf{r})$ and $K(\mathbf{r})$ are comparable with that of $\rho(\mathbf{r})$, with maxima at the nuclei positions and a saddle point between them, with $K(\mathbf{r})$ presenting a more pronounced spatial change than $G(\mathbf{r})$. In the case of $\nabla^2 G(\mathbf{r})$ also presents the same shape as $\rho(\mathbf{r})$ with no special structure within the bonding region, in contrast, $\nabla^2 K(\mathbf{r})$ has a shell structure in the neighborhood of the bond critical point (BCP). The Basis set effect is important for the accurate description of the interatomic region of the hydrogen molecule, whereas STO gives smooth curves, GTO produces additional unphysical oscillations. With STO, it is possible to observe a $K(\mathbf{r})$ concentration around the BCP, with two minima (around -0.5 and 0.5) and a saddle point (at zero). These features are similar to those that characterize a covalent bond when it is described by $\nabla^2 \rho(\mathbf{r})$. [58] Based on the observed changes of $\nabla^2 K(\mathbf{r})$ within the bonding region, it is possible to say that the stabilization of a covalent bond is originated by the concentration of both, electron and kinetic energy densities.

Another perspective that illustrates how the kinetic energy evolves during the formation of the hydrogen molecule is presented qualitatively in Figure 4 (at CCSD/aug-cc-pV5Z theoretical level), where the internuclear distance (Δr, in Å) is zero at the equilibrium structure. To obtain the exact behavior of $\nabla^2 K(\mathbf{r})$ during the formation of the hydrogen molecule, it is necessary to perform CASSCF/STO calculations which are not accessible, but the valence region features are similar with GTO basis functions, as has been shown in the previous section. When $\Delta r = 3.5$ Å, the contours are practically spherical with a valence $K(\mathbf{r})$ concentration shell, α_1, surrounding an internal depletion region. At $\Delta r = 3.0$ Å, both α_1 concentration shells start to polarize as the hydrogen nuclei approach, along with an increase of kinetic energy concentration at the internuclear region. At $\Delta r = 2.0$ Å, the concentration shells coalesce to form an external molecular concentration shell, δ_1, which allows the contact of the depletion shells of both atoms. A similar behaviour has been reported for the most outer shells of $K(\mathbf{r})$ in the formation of covalent bonds. [32;33] Note that between $\Delta r = 0.2$ Å and the equilibrium distance, $K(\mathbf{r})$ goes from being locally depleted to locally concentrated at the internuclear region. Throughout this process, an external molecular $K(\mathbf{r})$ concentration shell (δ_1) is formed and this shell ends as an enveloping region of kinetic energy concentration for both hydrogen nuclei.

3.4 Diatomic molecules

In order to confirm that the previous behavior is general, we analyzed the $\nabla^2 K(\mathbf{r})$ contour diagrams (Figure 6) of N_2, *CO* and *LiF* molecules, which are archetypes of the covalent, polar covalent and ionic bond respectively.

From table 2, it is known that nitrogen has two kinetic energy concentration shells, α_1 and α_2, one associated with the core and the other with the valance. During the formation of the nitrogen molecule, the valence shell of both nitrogen atoms fuses to form a symmetric molecular shell, δ_2, along with the merge of the outer depletion shells that cover both cores, as shown in Fig-

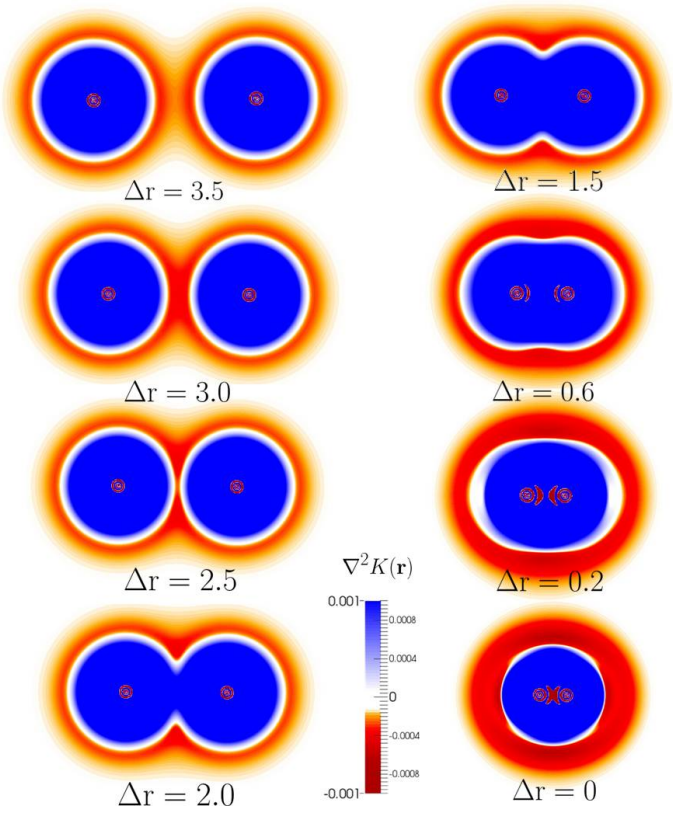

Fig. 4 Evolution of the $\nabla^2 K(\mathbf{r})$ as the Hydrogen atoms approach. The white contours represent nodes of the $\nabla^2 K(\mathbf{r})$

ure 6. Finally, the inner concentration and depletion shells are slightly polarized but separated.

In the case of polar molecules, as *CO*, it is possible to observe that the less electronegative atom presents a stronger perturbation in its shells. The α_2 valence shell of each isolated atom combines to form an asymmetric δ_2 molecular shell. In the vicinity of the carbon atom, the outer depletion shell is larger than the concentration shell. The combination of α_1 core shells also depicts a disproportionate distribution within the internuclear region. The bond critical point for the *CO* is found within the α_1 shell of the carbon atom.

In the case of *LiF*, as a consequence of the charge transfer from the Lithium to the Fluorine atom, the second charge concentration shell of the Lithium atom is no longer observed at the equilibrium distance, as described by Hernández-Trujillo and Bader.[59] A similar process is carried out with the valence shell concentration of $K(\mathbf{r})$ of the Lithium atom. The remaining shell (α_1) of the Li atom merges with the α_2 shell of the fluorine atom to form the molecular envelope shell of kinetic energy concentration δ_2. In this case, the critical point is found in the region of kinetic energy depletion of the Lithium atom. The inner shells of Florine atom remain unaltered. It is possible to say that every molecule has an external concentration shell of HKED that covers the whole molecule. Additionally, a covalent or a polar covalent molecule is characterized by a internuclear concentration of $K(\mathbf{r})$, whereas ionic interactions has a depletion of $K(\mathbf{r})$ between the nuclei. It is worth to mention that the type basis set effect are significantly less pronounced for bonding between heavy atoms than for the hydrogen bonding.

3.5 Organic molecules

To further expand our study, we analyzed the behavior of $\nabla^2 K(\mathbf{r})$ in particular cases of single, double, triple, and aromatic carbon-carbon bonds. Figure 7 shows the profile of $\nabla^2 K(\mathbf{r})$ along the C-C internuclear axis of ethane, ethylene, acetylene and benzene. The C-C bond presents two internuclear $K(\mathbf{r})$ concentrations connected by a saddle point similar to that presented in the symmetric diatomic molecules, H_2 and N_2. The four profiles have the same shape that differs in the width of saddle point and the value of the $K(\mathbf{r})$ concentration. The width decreases from the single (0.612 a.u.) to the triple (0.112 a.u.) bond while the magnitude of the concentration increases in the same direction, from -37.7 a.u. in ethane to -43.3 a.u. in acetylene, correlating with the bond order. Also, it is possible to observe that each organic molecule is surrounded by a δ_2 shell of $K(\mathbf{r})$ concentration.

3.6 Weak interactions

Finally, the C_6H_6/C_6H_6 and CH_4/CH_4 dimers were studied as examples of systems where weak interactions are presented. The first case is a prototype case of π-π stacking and the latter a prototype of van der Waals interacting molecules. Figure 8 shows the envelopes maps of each organic dimer. In the case of the benzene dimer, the concentration δ_2 shells of both benzene merge producing an intermolecular surface. Moreover, this $\nabla^2 K(\mathbf{r})$ surface matches with the intermolecular bond critical points and the NCI surface observed for the same dimer. In the case of methane, the δ_2 molecular shell is localized around the C-H bonds. It can be seen from Figure 8 that similarly to the benzene dimer, the δ_2 of the methane molecules merge to produce an intermolecular surface.

4 Conclusions

We have explored the topographic behavior of the HKED and its Laplacian for a variety of chemical scenarios, going from atoms to diatomic molecules and from strong covalent bonded atoms to weak interacting molecular systems. Though simple and readily interpretable, we observed that $G(\mathbf{r})$ and $\nabla^2 G(\mathbf{r})$ do not reveal substantial chemical information. On the contrary, $K(\mathbf{r})$ and $\nabla^2 K(\mathbf{r})$ unveil a structured shell behavior in atoms, which allows the observation of changes associated with the formation of bonds and presence of chemical interactions. Particularly, the atomic shells of $\nabla^2 K(\mathbf{r})$ melt when forming a covalent bond yielding an

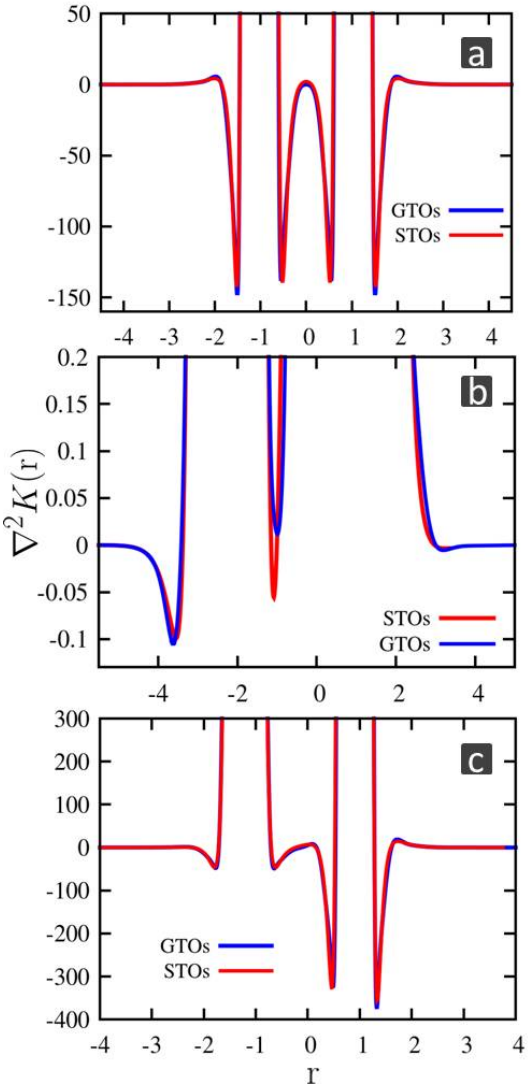

Fig. 5 Profiles of $\nabla^2 K(\mathbf{r})$ along the internuclear axis of a) N_2, b) CO and c) LiF. These molecules were taken as archetypal cases of covalent, polar covalent and ionic bindings respectively

intramolecular dilution region (in which the nuclei are embedded) and an external concentration region (that envelopes the interacting atoms). Besides, One can observe two internuclear $K(\mathbf{r})$ concentrations connected by a saddle point. In the case of a ionic bond, the $\nabla^2 K(\mathbf{r})$ atomic shells do not fuse and the external concentration is not observed. We found that, when it comes to intermolecular interactions, the molecular external concentration regions come into contact and coalesce without losing their form, avoiding the contact of the inner shells. The inherent ambiguity of the quantum KED restricts most of its definitions from a classical (or even unique) interpretation nevertheless, in light of this work we have shown that the analysis of the local changes of $\nabla^2 K(\mathbf{r})$ opens the possibility to an energetic description of weakly interacting systems.

5 Acknowledgements

The authors acknowledge PAPIIT/DGAPA/UNAM (Grant IN202717) for financial support, and DGTIC-UNAM (LANCAD-UNAM-DGTIC-194) for computer time. We thank Prof. James Anderson for his valuable comments on this manuscript.

References

1 H. Hellmann, *Zeitschrift für Physik*, 1933, **85**, 180–190.
2 R. E. Pierls, *Quantum Theory of Solids*, Clarendon Press: Oxford, 1995, ch. 5.
3 J. R. Platt, in *The Chemical Bond and the Distribution of Electrons in Molecules*, Springer Berlin Heidelberg, Berlin, Heidelberg, 1961, pp. 173–281.
4 K. Ruedenberg, *Rev. Mod. Phys.*, 1962, **34**, 326–376.
5 M. Feinberg, K. Ruedenberg and E. L. Mehler, *E. L. Mehler*, Academic Press, 1970, vol. 5, pp. 27 – 98.
6 M. J. Feinberg and K. Ruedenberg, *The Journal of Chemical Physics*, 1971, **54**, 1495–1511.
7 M. J. Feinberg and K. Ruedenberg, *The Journal of Chemical Physics*, 1971, **55**, 5804–5818.
8 K. Ruedenberg, in *The Nature of the Chemical Bond, an Energetic View*, ed. O. Chalvet, R. Daudel, S. Diner and J. P. Malrieu, Springer Netherlands, Dordrecht, 1975, pp. 223–245.
9 K. Ruedenberg and M. W. Schmidt, *Journal of Computational Chemistry*, 2006, **28**, 391–410.
10 W. Kutzelnigg, *Angewandte Chemie International Edition in English*, 1973, **12**, 546–562.
11 W. Kutzelnigg and W. H. E. Schwarz, *Phys. Rev. A*, 1982, **26**, 2361–2367.
12 M. W. Schmidt, J. Ivanic and K. Ruedenberg, in *The Physical Origin of Covalent Bonding*, John Wiley Sons, Ltd, 2014, ch. 1, pp. 1–68.
13 J. C. Slater, *The Journal of Chemical Physics*, 1933, **1**, 687–691.
14 R. P. Feynman, *Phys. Rev.*, 1939, **56**, 340–343.
15 C. A. C. A. Coulson, *Valence*, London ; New York : Oxford University Press, 2nd edn, 1961.
16 R. F. W. Bader, *The Journal of Physical Chemistry A*, 2011, **115**, 12667–12676.
17 R. F. W. Bader, *Foundations of Chemistry*, 2011, **13**, 11–37.
18 G. B. Bacskay, S. Nordholm and K. Ruedenberg, *The Journal of Physical Chemistry A*, 2018, **122**, 7880–7893.
19 J. S. Anderson, P. W. Ayers and J. I. Hernandez, *Journal of Physical Chemistry A*, 2010, **114**, 8884–8895.
20 L. Cohen, *The Journal of Physical Chemistry A*, 2011, **115**, 12919–12923.

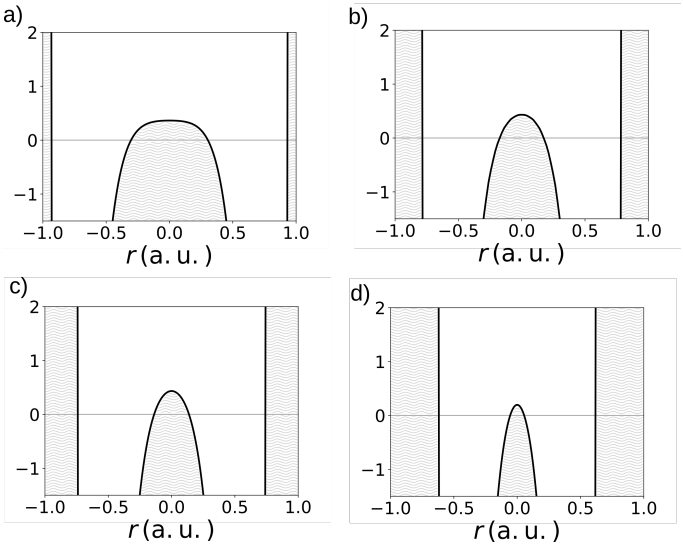

Fig. 7 Profile of $\nabla^2 K(\mathbf{r})$ of C−C bond in a) ethane b) benzene c) ethylene d) acetylene.

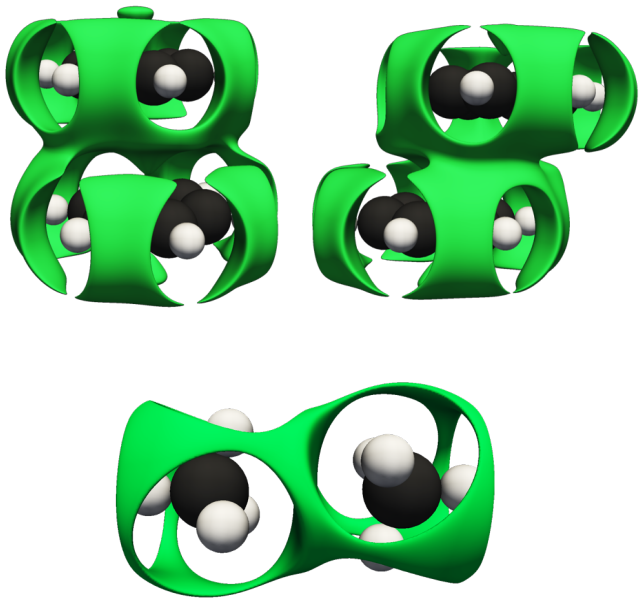

Fig. 8 The $\nabla^2 K(\mathbf{r})$ isosurface of the benzene dimer in a sandwich conformation (top) and the $\nabla^2 K(\mathbf{r})$ isosurface of the methane dimer (bottom)

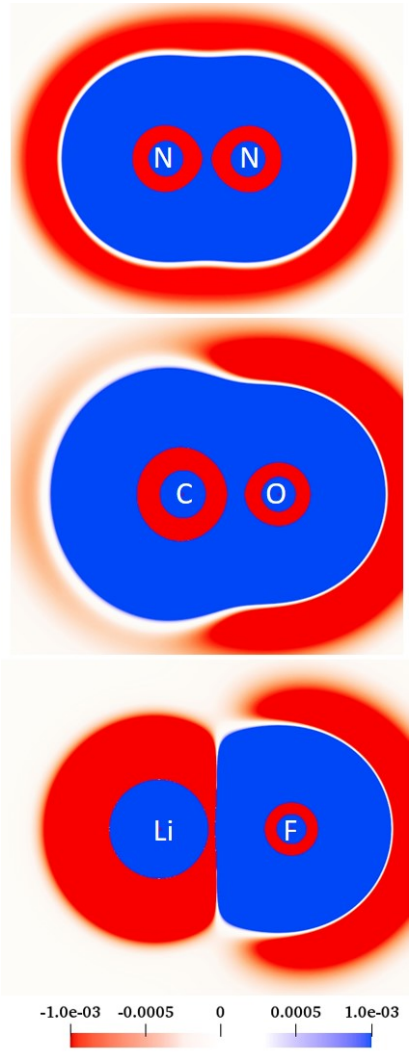

Fig. 6 $\nabla^2 K(\mathbf{r})$ of the diatomic molecules N_2, CO and LiF with STO basis set

21 G. B. Bacskay and S. Nordholm, *Journal of Physical Chemistry A*, 2013, **117**, 7946–7958.

22 H. Jacobsen, *Dalton Transactions*, 2010, **39**, 5426–5428.

23 H. Jacobsen, *Physical Chemistry Chemical Physics*, 2013, **15**, 5057–5066.

24 F. Della Sala, E. Fabiano and L. A. Constantin, *International Journal of Quantum Chemistry*, 2016.

25 R. F. W. Bader and H. J. T. Preston, *International Journal of Quantum Chemistry*, 1969, **3**, 327–347.

26 S. Noorizadeh, *Chemical Physics Letters*, 2016, **652**, 40–45.

27 H. Nozaki, K. Ichikawa and A. Tachibana, *International Journal of Quantum Chemistry*, 2016, **116**, 504–514.

28 H. Schmider and A. Becke, *Journal of Molecular Structure: THEOCHEM*, 2000, **527**, 51 – 61.

29 H. Jacobsen, *Dalton Trans.*, 2010, **39**, 5426–5428.

30 V. F. Weisskopf, *Science*, 1975, **187**, 605–612.

31 M. Torrent-Sucarrat, S. Liu and F. De Proft, *The Journal of Physical Chemistry A*, 2009, **113**, 3698–3702.

32 A. Tachibana, *The Journal of Chemical Physics*, 2001, **115**,

3497–3518.

33 P. Szarek, Y. Sueda and A. Tachibana, *The Journal of chemical Physics*, 2012.

34 R. Bader, *Atoms in Molecules: A Quantum Theory*, Clarendon Press, 1994.

35 P. L. A. Popelier, in *On Quantum Chemical Topology*, ed. R. Chauvin, C. Lepetit, B. Silvi and E. Alikhani, Springer International Publishing, Cham, 2016, pp. 23–52.

36 R. F. W. Bader and P. M. Beddall, *The Journal of Chemical Physics*, 1972, **56**, 3320–3329.

37 P. L. A. Popelier, in *The QTAIM Perspective of Chemical Bonding*, John Wiley Sons, Ltd, 2014, ch. 8, pp. 271–308.

38 V. Tognetti and L. Joubert, *Phys. Chem. Chem. Phys.*, 2014, **16**, 14539–14550.

39 P. Popelier, *Atoms in Molecules. An Introduction*, Pearson Education, United Kingdom, 2000.

40 R. F. Bader and P. M. Beddall, *The Journal of Chemical Physics*, 1972, **56**, 3320–3329.

41 R. F. W. Bader, P. J. MacDougall and C. D. H. Lau, *Journal of the American Chemical Society*, 1984, **106**, 1594–1605.

42 R. F. W. Bader, R. J. Gillespie and P. J. MacDougall, *Journal of the American Chemical Society*, 1988, **110**, 7329–7336.

43 A. D. Becke and K. E. Edgecombe, *The Journal of Chemical Physics*, 1990, **92**, 5397–5403.

44 E. Cancès, R. Keriven, F. Lodier and A. Savin, *Theoretical Chemistry Accounts*, 2004, **111**, 373–380.

45 R. A. Boto, J. Contreras-García, J. Tierny and J.-P. Piquemal, *Molecular Physics*, 2016, **114**, 1406–1414.

46 D. Sundholm, H. Fliegl and R. J. F. Berger, *Wiley Interdisciplinary Reviews: Computational Molecular Science*, 2016, **6**, 639–678.

47 J. E. Barquera-Lozada, *International Journal of Quantum Chemistry*, 2019, **119**, e25848.

48 C. F. Matta and R. J. Boyd, in *An Introduction to the Quantum Theory of Atoms in Molecules*, John Wiley Sons, Ltd, 2007, ch. 1, pp. 1–34.

49 A. Martín Pendás, E. Francisco, A. Gallo Bueno, J. M. Guevara Vela and A. Costales, in *Emergent Scalar and Vector Fields in Quantum Chemical Topology*, ed. R. Chauvin, C. Lepetit, B. Silvi and E. Alikhani, Springer International Publishing, Cham, 2016, pp. 131–150.

50 A. M. Pendás and E. Francisco, 2018.

51 R. F. W. Bader, *The Journal of Chemical Physics*, 1980, **73**, 2871–2883.

52 Y. Zhao and D. G. Truhlar, *Theoretical Chemistry Accounts*, 2008, **120**, 215–241.

53 E. J. Baerends, T. Ziegler, A. J. Atkins, J. Autschbach, D. Bashford, O. Baseggio, A. Bérces, F. M. Bickelhaupt, C. Bo, P. M. Boerritger, L. Cavallo, C. Daul, D. P. Chong, D. V. Chulhai, L. Deng, R. M. L[This journal is © The Royal Society of Chemistry [year]] Faassen, A. Ghysels, A. Giammona, S. J. A. van Gisbergen, A. Goez, A. W. Götz, S. Gusarov, F. E. Harris, P. van den Hoek, Z. Hu, C. R. Jacob, H. Jacobsen, L. Jensen, L. Joubert, J. W. Kaminski, G. van Kessel, C. König, F. Kootstra, A. Kovalenko, M. Krykunov, E. van Lenthe, D. A. McCormack, A. Michalak, M. Mitoraj, S. M. Morton, J. Neugebauer, V. P. Nicu, L. Noodleman, V. P. Osinga, S. Patchkovskii, M. Pavanello, C. A. Peeples, P. H. T. Philipsen, D. Post, C. C. Pye, H. Ramanantoanina, P. Ramos, W. Ravenek, J. I. Rodríguez, P. Ros, R. Rüger, P. R. T. Schipper, D. Schlüns, H. van Schoot, G. Schreckenbach, J. S. Seldenthuis, M. Seth, J. G. Snijders, M. Solà, S. M., M. Swart, D. Swerhone, G. te Velde, V. Tognetti, P. Vernooijs, L. Versluis, L. Visscher, O. Visser, F. Wang, T. A. Wesolowski, E. M. van Wezenbeek, G. Wiesenekker, S. K. Wolff, T. K. Woo and A. L. Yakovlev, *ADF2017, SCM, Theoretical Chemistry, Vrije Universiteit, Amsterdam, The Netherlands, https://www.scm.com*.

54 M. Kohout, DGrid, version 5.0, Dresden, 2017.

55 Gaussian 09, Revision A.02, M. J. Frisch, G. W. Trucks, H. B. Schlegel, G. E. Scuseria, M. A. Robb, J. R. Cheeseman, G. Scalmani, V. Barone, G. A. Petersson, H. Nakatsuji, X. Li, M. Caricato, A. Marenich, J. Bloino, B. G. Janesko, R. Gomperts, B. Mennucci, H. P. Hratchian, J. V. Ortiz, A. F. Izmaylov, J. L. Sonnenberg, D. Williams-Young, F. Ding, F. Lipparini, F. Egidi, J. Goings, B. Peng, A. Petrone, T. Henderson, D. Ranasinghe, V. G. Zakrzewski, J. Gao, N. Rega, G. Zheng, W. Liang, M. Hada, M. Ehara, K. Toyota, R. Fukuda, J. Hasegawa, M. Ishida, T. Nakajima, Y. Honda, O. Kitao, H. Nakai, T. Vreven, K. Throssell, J. A. Montgomery, Jr., J. E. Peralta, F. Ogliaro, M. Bearpark, J. J. Heyd, E. Brothers, K. N. Kudin, V. N. Staroverov, T. Keith, R. Kobayashi, J. Normand, K. Raghavachari, A. Rendell, J. C. Burant, S. S. Iyengar, J. Tomasi, M. Cossi, J. M. Millam, M. Klene, C. Adamo, R. Cammi, J. W. Ochterski, R. L. Martin, K. Morokuma, O. Farkas, J. B. Foresman, and D. J. Fox, Gaussian, Inc., Wallingford CT, 2016.

56 AIMAll (Version 17.11.14), Todd A. Keith, TK Gristmill Software, Overland Park KS, USA, 2017 (aim.tkgristmill.com).

57 G. B. Bacskay and S. Nordholm, *The Journal of Physical Chemistry A*, 2017, **121**, 9330–9345.

58 F. Cortés-Guzmán, R. M. Gómez, T. Rocha-Rinza, M. A. Sánchez-Obregón and J. M. Guevara-Vela, *The Journal of Physical Chemistry A*, 2011, **115**, 12924–12932.

59 J. Hernández-Trujillo and R. F. Bader, *The Journal of Physical Chemistry A*, 2000, **104**, 1779–1794.

Table 1 Numerical values (in a.u.) associated to $K(\mathbf{r})$ for atoms from H to Ca. α_i and β_i are situated right below their corresponding radius (r_{α_i} or r_{β_i})

Atom	j_1	r_{α_1}/α_1	j_2	r_{β_1}/β_1	j_3	r_{α_2}/α_2	j_4	r_{β_2}/β_2	j_5	r_{α_3}/α_3
H	2.022	2.4575								
		-2.22E-004								
He	1.1975	1.4835								
		-0.004598963								
Li	0.74	0.889	1.9145	2.313	5.0925	5.9195				
		-0.05380428		6.05E-004		-5.30E-006				
Be	0.542	0.6485	1.1635	1.4385	3.3975	3.9695				
		-0.264151578		0.012065785		-6.95E-005				
B	0.4285	0.514	0.879	1.085	2.531	2.9445				
		-0.882838128		0.052340384		-2.96E-004				
C	0.377	0.4315	0.555	0.7505	2.5115	2.9195				
		-0.996473025		0.552027642		-0.000466994				
N	0.327	0.3695	0.4525	0.62	2.067	2.403				
		-1.653037823		1.42594732		-0.001230441				
O		0.335		0.455	1.9505	2.2345				
		4.342168859		6.166930487		-0.002003628				
F		0.2995		0.3865	1.6905	1.9495				
		10.629996983		12.864759689		-0.004245983				
Ne		0.2715		0.3365	1.4965	1.73				
		21.705691158		24.240140133		-0.007829006				
Na	1.2325	1.42	2.6865	3.087	5.513	6.384				
		-0.026552014		2.05E-004		-4.05E-006				
Mg	1.067	1.2245	1.9145	2.2715	4.2135	4.8945				
		-0.057480791		0.002196188		-3.14E-005				
Al	0.937	1.0685	1.5835	1.8695	3.306	3.814				
		-0.108540346		0.006755313		-1.12E-004				
Si	0.839	0.9455	1.2245	1.5075	3.638	4.237				
		-0.173402815		0.045550471		-8.88E-005				
P	0.7625	0.8545	1.0695	1.317	3.036	3.458				
		-0.259898978		0.09835536		-2.54E-004				
S	0.699	0.7785	0.95	1.174	2.6885	3.043				
		-0.362872599		0.192199459		-5.30E-004				
Cl	0.652	0.706	0.793	1.0195	2.5085	2.8415				
		-0.308522777		0.556588966		-0.001018525				
Ar	0.6105	0.6525	0.714	0.9295	2.271	2.5735				
		-0.313183175		0.9332493		-0.001808983				
K	0.582	0.606	0.631	0.846	1.976	2.243	3.852	4.372	6.8735	7.852
		-0.132873486		1.636050874		-0.004529514		0.000044386		-0.0000017
Ca		0.5635		0.7735	1.7655	1.9865	2.8215	3.2785	5.4325	6.26

Table 2 Numerical values (in a.u.) associated to $\nabla^2 K(\mathbf{r})$ for atoms from H to Ca. α_i and β_i are situated right below their corresponding radius (r_{α_i} or r_{β_i})

ATOM	j_1	r_{α_1}/α_1	j_2	r_{β_1}/β_1	j_3	r_{α_2}/α_2	j_4	r_{β_2}/β_2	j_5	r_{α_3}/α_3	j_6
He	1.73812	1.99568									
		-0.00474									
Li	1.10792	1.28328	2.90536	3.3328	7.06468	7.09756					
		-0.13656		0.00019		-0.00000007					
Be	0.80652	0.93256	1.85868	2.12172	4.69732	4.72472					
		-1.48945		0.0077		-0.00000232					
B	0.63116	0.7298	1.34356	1.56276	3.86436	4.03972					
		-8.87347		0.0952		-0.00004251					
C	0.51608	0.59828	1.03668	1.223	3.26156	3.59584					
		-36.28196		0.67747		-0.00022404					
N	0.43936	0.50512	0.83392	0.99284	2.77932	3.06428					
		-115.4789		3.38673		-0.00080532					
O	0.37908	0.43936	0.69692	0.83392	2.43956	2.71904					
		-309.9434		12.68841		-0.00198891					
F	0.33524	0.38456	0.5928	0.71336	2.182	2.44504					
		-729.8511		40.7264		-0.00469635					
Ne	0.30236	0.3462	0.51608	0.6202	1.96828	2.19844					
		-1554.024		115.3129		-0.01067165					
Na	0.26948	0.31332	0.45032	0.54896	1.65592	1.86416	3.58488	3.99588	6.8674	6.87836	
		-3290.048		303.4992		-0.04704581		0.00011116		-0.00000001	
Mg	0.24756	0.28592	0.40648	0.49416	1.40932	1.5792	2.68616	2.99852	5.33848	5.34944	
		-6266.933		677.6692		-0.1894483		0.00162165		-0.00000065	
Al	0.22564	0.25852	0.36812	0.45032	1.22848	1.37096	2.2368	2.56012	5.05352	5.12476	
		-11104.17		1382.663		-0.5860227		0.00804356		-0.00000334	
Si	0.2092	0.24208	0.33524	0.41196	1.08052	1.20656	1.86964	2.12172	4.71376	4.75212	
		-19238.02		2713.407		-1.739363		0.0366997		-0.00000417	
P	0.19276	0.22564	0.30784	0.37908	0.96544	1.086	1.634	1.8806	4.06164	4.1	
		-32170.12		5093.814		-4.236046		0.1260265		-0.00001881	
S	0.1818	0.2092	0.28592	0.35168	0.87776	0.98188	1.45316	1.68332	3.6068	3.94656	
		-51979.43		9124.594		-9.381371		0.3504405		-0.00024672	
Cl	0.17084	0.19824	0.264	0.32976	0.80104	0.89968	1.3052	1.50796	3.24512	3.53008	
		-80821.44		15732.41		-19.57989		0.8840574		-0.00061423	
Ar	0.15988	0.1818	0.24756	0.30784	0.73528	0.82296	1.18464	1.37096	2.94372	3.24512	
		-122721.5		26195.35		-38.80572		2.038936		-0.0014882	
K	0.14892	0.17632	0.23112	0.28592	0.68048	0.76816	1.08052	1.2504	2.57108	2.84508	4.94392
		-180571		42052.48		-70.42233		4.391843		-0.00583386	
Ca	0.14344	0.16536	0.21468	0.26948	0.63116	0.70788	0.98736	1.14628	2.27516	2.52176	3.78764
		-269663.3		65878.15		-129.4737		9.250498		-0.01719778	